ACS APPLIED MATERIALS & INTERFACES

Research Article

www.acsami.org

# Low-Cost Electrospun Highly Crystalline Kesterite $Cu_2ZnSnS_4$ Nanofiber Counter Electrodes for Efficient Dye-Sensitized Solar Cells

Sawanta S. Mali,[†] Pramod S. Patil,[‡] and Chang Kook Hong*,[†]

[†]School of Applied Chemical Engineering, Chonnam National University, Gwangju, 500-757 South Korea

[‡]Thin Film Materials Laboratory, Department of Physics, Shivaji University, Kolhapur, India 416 004

Supporting Information

**ABSTRACT:** In the present investigation, kesterite $Cu_2ZnSnS_4$ (CZTS) nanofibers were obtained by electrospinning process using polyvinylpyrrolidone (PVP) and cellulose acetate (CA) solvent separately. The synthesized CZTS nanofibers were characterized using thermogravimetric analysis (TGA), optical absorption, X-ray powder diffraction (XRD), field-emission scanning electron microscopy (FESEM), micro-Raman spectroscopy, high-resolution transmission electron microscopy (HRTEM), and X-ray photoelectron spectroscopy (XPS). Our results showed that the PVP synthesized CZTS nanofibers are a single crystalline while CA assisted CZTS nanofibers are polycrystalline in nature. The optical properties demonstrated that the prepared nanofibers have strong absorption in 300−550 nm range with band gap energy of 1.5 eV. The X-ray and micro-Raman analysis revealed that synthesised nanofibers showing pure phase kesterite CZTS. Further the synthesized CZTS nanofibers were used as counter electrodes for dye-sensitized solar cells (DSSCs). Our results indicate that, PVP-CZTS and CA-CZTS counter electrode based DSSC shows 3.10% and 3.90% respectively. The detailed interfaces of these counter electrodes and DSSCs were analyzed by electrochemical impedance spectroscopic (EIS) measurements for analysis of such high power conversion efficiency. The present study will be helpful for alternative counter electrode for Pt counter electrodes in DSSCs application. We believe that our synthetic method will be helpful for low-cost and efficient thin film photovoltaic technology.

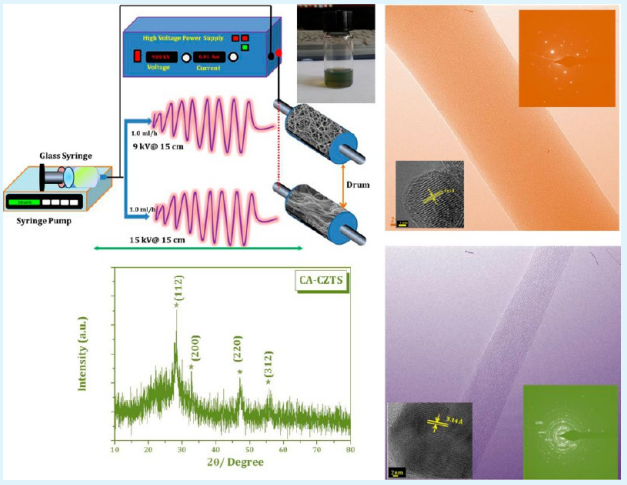


**KEYWORDS:** *PVP-CZTS, CA-CZTS nanofibers, DSSC counter electrodes, 3.9 percent efficiency*

## 1. INTRODUCTION

Low-band-gap quaternary and pentanary semiconductors, such as $Cu(In_{1-x},Ga_x)Se_2$ (CIGS), $Cu_2ZnSnS_4$ (CZTS), and $Cu_2ZnSnSSe_4$ (CZTSSe), are of great interest because of their potential application as light absorbing materials in thin film photovoltaic technology. However, the preparation of indium and gallium based quaternary/pentanary semiconductors are not abundant and not low cost. Therefore, the production cost could be increased high and also these materials are not biocompatible. On the other hand, CZTS and CZTSSe have been considered as an alternative to CIGS as the absorber layers because of their easy processing ability, high efficiency at low cost, and environmental eco-friendliness. Moreover, CZTS is abundance, it has good optical absorption coefficient ($>1 \times 10^4$ $cm^{-1}$) and suitable band gap energy (1.0 to 1.5 eV).[1−5] After the first report of Katagiri et al.,[1] CZTS has been synthesized by number of vacuum and nonvacuum techniques have been employed for the synthesis of CZTS.[6−14] Comparing these vacuum and nonvacuum techniques, the solution-processed nonvacuum technique is the ideal approach for the low-cost and large-scale synthesis.[15−20] In solution process, synthesis of $Cu_2ZnSn(S,Se)_4$ from hydrazine-based solution demonstrated 10.1% conversion efficiency,[21] whereas CZTS nanocrystal synthesized by hot-injection method shows 7.2% conversion efficiency.[22] Recently, 11.1% conversion efficiency has been reported by Todorov et al.,[23] which is the best so far.

Similarly, the structural relation between kesterite and stannite, wurtzkesterite and wurtzstannite, is that they have a similar unit cell but differ in the occupation of Cu, Zn and Sn cations. Kesterite and stannite type CZTS(Se) nanocrystals (NCs), nanosheets and nanowires have been extensively reported.[24,25] However, these techniques required post-annealing treatment such as sulfurization and selenization. On the other hand, nonvacuum solution process electrospinning methods are the most popular because of their simplicity, large scale production capability, and absence of vacuum process. With the help of electrospinning technique we can easily synthesize 1D nanofibers and nanowires.[26] Recently, synthesis of $TiO_2$ and ZnO

**Received:** October 17, 2013
**Accepted:** January 2, 2014
**Published:** January 2, 2014

  

**Scheme 1. Schematic Representation of Electrospinning Set up for the Synthesis of CZTS Nanofibers Using Different PVP and CA Polymers**

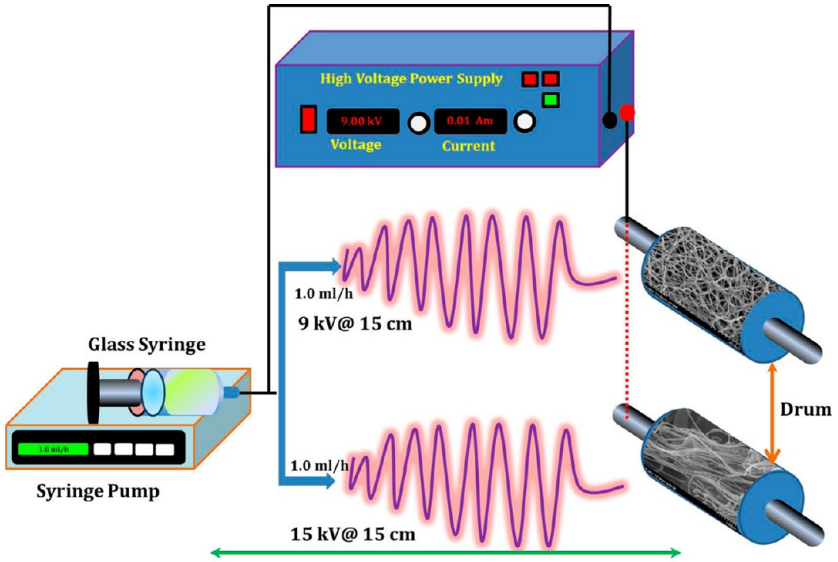


nanowires/nanofibers using electrospinning technique has been widely used.[27,28] However, there is no single report for the fabrication of CZTS nanofibers using polyvinylpyrrolidone (PVP) and cellulose acetate (CA) polymers by electrospining technique. Herein, we report a synthesis of CZTS nanofibers by using PVP and CA as the electrospinning medium. Because both polymeric medium (CA and PVP) have good electrospinnability and low cost.[28] Therefore, electrospinning using PVP and CA has been widely used for the synthesis of nanofibers/nanowires. Moreover, because of nontoxicity and eco-friendliness, these polymers are widely used for the synthesis of polymer−inorganic nanomaterial composites and their relative applications.

Nowadays, novel approaches are implementing in DSSCs technology like the combination of different chalocogenide counter electrodes and ZnO- or $TiO_2$-based DSSCs to fabricate dye sensitized solar cells (DSSCs) with a theoretical efficiency limitation well beyond that of single junction DSSCs.[29,30] Generally n-type DSSC are based on nanoporous $TiO_2$ as the photoanode has a considerable ∼12% conversion efficiency. On the other hand, there is no substantial development in p-type counter electrodes. Narrow band gap p-type semiconductors have opened a new way for the hybrid DSSCs technology. Recently some narrow band gaps p-type nanostructured semiconductor thin films have been successfully used as counter electrodes for DSSCs. Due to high cost and scarcity of CdTe and CIGS p-type semiconductor materials have become a challenge for DSSCs.

The Kesterite CZTS and relative quaternary materials can be used as an alternative to expensive Pt/FTO counter electrodes of Gratzel cell. In this investigation, we report a green, low-cost, and simple PVP and CA polymer assisted electrospinning technique for synthesis of CZTS nanofibers. Copper(II) chloride (CuCl), zinc(II) chloride ($ZnCl_2$), tin(IV) chloride pentahydrate ($SnCl_4{\cdot}5H_2O$) and thiourea ($CH_4N_2S$) were used as precursors of Cu, Zn, Sn, and S, respectively. Here PVP and CA were used as electrospinning medium for synthesis of single crystalline CZTS nanofibers and polycrystalline CZTS nanofibers respectively. Furthermore, the as-prepared PVP-CZTS and CA-CZTS nanofibers were annealed at 450 °C for 3 h in

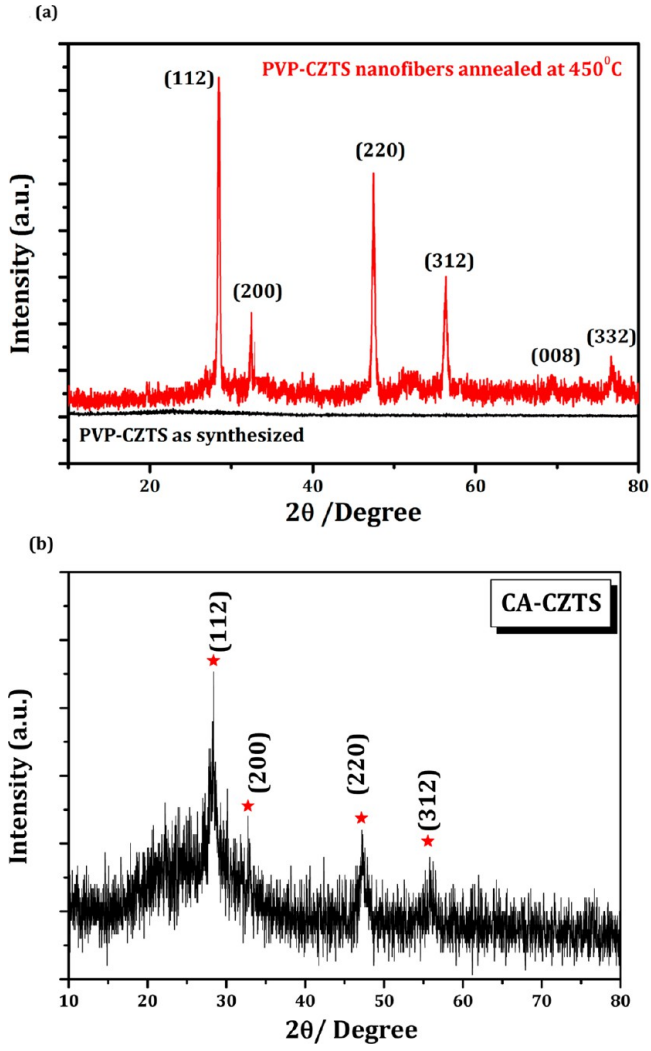


**Figure 1.** (a) XRD patterns of as synthesized PVP-CZTS (black color), PVP-CZTS nanofibers annealed at 450 °C (red color) and (b) CA-CZTS nanofibers annealed at 450 °C.


dx.doi.org/10.1021/am404586n | ACS Appl. Mater. Interfaces 2014, 6, 1688−1696

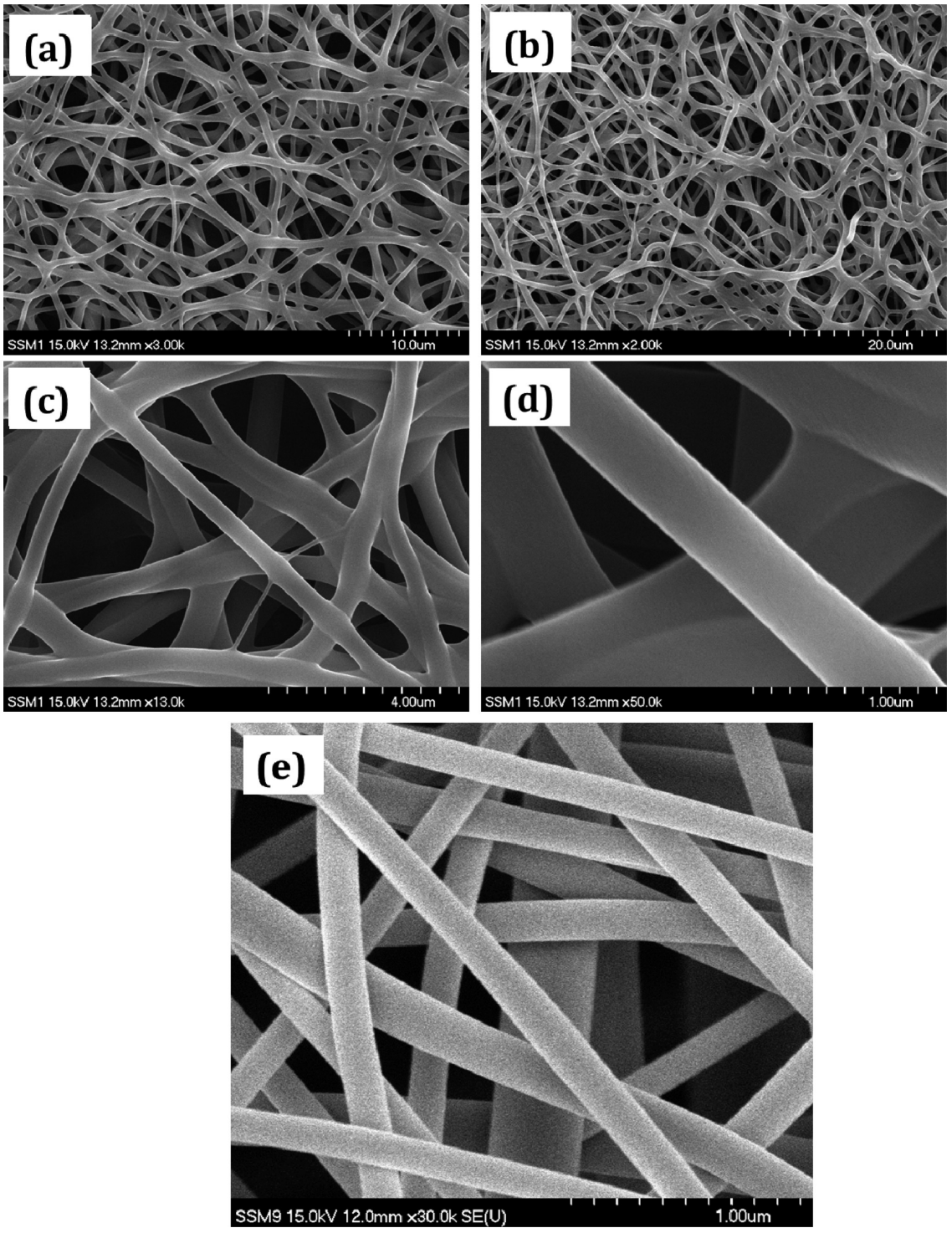


**Figure 2.** (a–d) FESEM images CZTS nanofibers synthesized in PVP solvent at different magnifications, (e) FESEM image of PVP-CZTS after annealing in nitrogen atmosphere.

nitrogen environment and characterized by different characterization techniques. Further, the synthesized CZTS nanofibers were used as counter electrodes for $TiO_2$ DSSC application. This present synthetic strategy will be helpful for low-cost efficient CZTS counter electrodes for DSSCs application.

## 2. MATERIALS AND METHODS

**2.1. Chemicals and Materials.** Polyvinylpyrrolidone (PVP) ((PVP K90, $M_W$ = 1300,000, Alfa Aesar), cellulose acetate (CA) (Mn 50,000, Aldrich), copper(II) chloride (CuCl) (Aldrich), zinc(II) chloride ($ZnCl_2$) tin(IV) (Aldrich) chloride pentahydrate ($SnCl_4{\cdot}5H_2O$) (Aldrich) and Thiourea ($CH_4N_2S$) (Aldrich) were used precursor for Cu, Zn, Sn, and S, respectively. The solvent acetone and ethanol were used a solvent (Daejung chemical).

**2.2. Preparation of PVP-CZTS and CA-CZTS Feeding Solutions.** Initially, 4 mg (2 mmol) of CuCl, 1.8 mg (1 mmol) of $ZnCl_2$, 3.8 mg (1 mmol) of $SnCl_4{\cdot}5H_2O$, and 18.3 mg (12 mmol) of thiourea were dissolved into 10 wt % CA solution. The CA solution is prepared from acetone:water (1:9 v:v) under vigorous stirring.

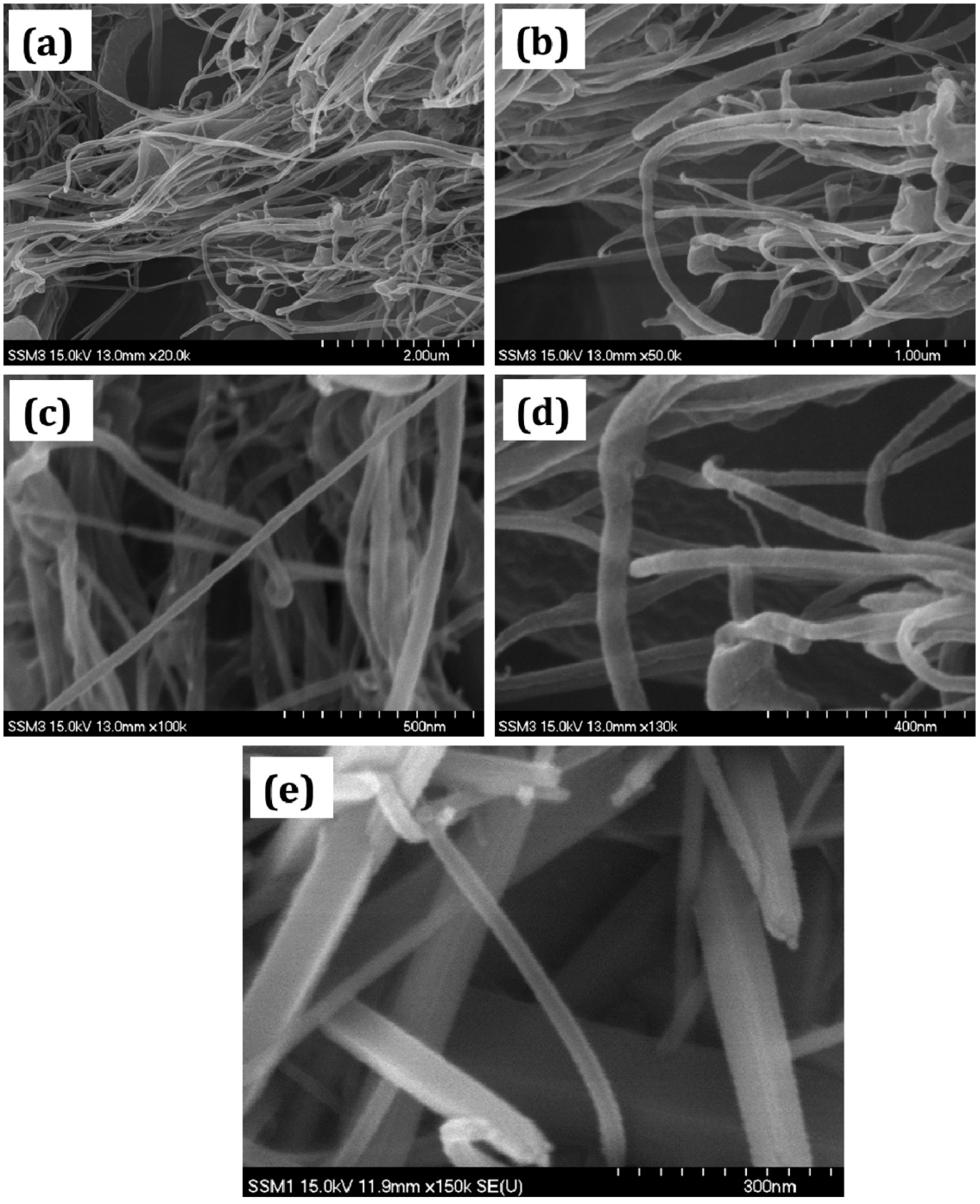


**Figure 3.** (a–d) FESEM images CZTS nanofibers synthesized in CA solvent at different magnifications, (e) FESEM image of CA-CZTS after annealing in nitrogen atmosphere.

For PVP-CZTS solution, we have kept all preparative parameters (Cu, Zn, Sn, and S) the same and dissolved into 10 wt % PVP solution prepared from ethanol:water (1:9 v:v).

**2.3. Preparation of Single-Crystalline and Polycrystalline CZTS Nanofibers.** The above prepared CA-CZTS and PVP-CZTS nanofibers were deposited using an electrospinning technique as shown in Scheme 1. More detailed experimental conditions are available in our previous report.[28] In the present experiments, we have used 15 and 9 kV potential for the deposition of PVP-CZTS and CA-CZTS nanofibers, respectively. The feeding rate 1.0 mL/h was kept constant for both samples.

The obtained PVP-CZTS and CA-CZTS samples were annealed at 450 °C for 3 h (heating rate: 2 °C $min^{-1}$) under nitrogen atmosphere using programmable tube furnace and used for further characterizations. Please note that we have prepared fresh electrospinning solutions prepared before each experiment. The annealing temperatures of both synthesized nanofibers were determined using TGA-DTA analysis (see the Supporting Information, Figures S1 and S2).

**2.4. DSSC Device Fabrication and Its Performance.** The preparation of $TiO_2$ photoelectrodes were prepared from standard doctor blade technique using commercial $TiO_2$ paste (Dyesol 18NRT, Dyesol)) followed by annealing and dye loading (ethanolic 0.5 mM N719 dye solution (Dyesol)). The CZTS/FTO counter electrodes were prepared by direct deposition of CZTS nanofibers onto FTO-coated glass substrate by electrospinning technique followed by annealing at 450 °C for 3 h in a nitrogen environment. For comparison,

Pt-coated FTO was used as a counter electrode. More details of fabrication of DSSC devices and sealing are available elsewhere.[31]

**2.5. Characterizations.** Structural characterizations of the synthesized CZTS nanofibers were characterized by X-ray diffraction (XRD) measurements (model D/MAX Uitima III XRD spectrometer, Rigaku, Japan) $\lambda$ = 1.5410 Å. The field-emission scanning electron microscopy (FESEM) and transmission electron microscopy (TEM), etc., microscopic techniques were used for morphological studies. The sample preparation for TEM, high-resolution transmission electron microscopy (HRTEM), and selected area electron diffraction (SAED) pattern was as per our earlier paper.[28] Thermal analysis of as synthesized CA-CZTS and PVP-CZTS nanofiber samples were carried out using a thermogravimetric and differential thermal analysis TG-DTA thermal analyzer ( model Perkin Elmer Pyris Diamond) in a nitrogen atmosphere. The heating rate and nitrogen gas flow rate were kept 10 °C $min^{-1}$ and 50 mL $min^{-1}$, respectively. The elemental information regarding the deposited CZTS nanofiber samples was analyzed using an X-ray photoelectron spectrometer (XPS). The optical absorption spectra of CZTS nanofibers were recorded using a UV-vis spectrometer (Varian, CARY, 300 Conc.). In typical measurements, CZTS nanofibers were well-dispersed in toluene solution by using ultra sonication treatment.

The fabricated DSSC devices were tested under 100 mW $cm^{-2}$ illumination. Electrochemical impedance spectroscopy (EIS) was conducted using electrochemical workstation (model Iviumstat Ivium Technologies B.V., Eindhoven, the Netherlands).[26] The EIS data was analyzed using Z-view 2.8d software for equivalent circuit. The catalytic activity of PVP-CZTS and CA-CZTS counter electrodes were tested using cyclic voltammetry (CV) experiments in $I_3^-/I^-$ redox couple with three electrodes system (see the Supporting information, Figure S3).

## 3. RESULTS AND DISCUSSION

The structural properties of the as synthesized and annealed CZTS samples were recorded using XRD and are shown in Figure 1. Figure 1a show the indexed XRD patterns for the as synthesized PVP-CZTS nanofibers and annealed at 450 °C in nitrogen atmosphere. XRD pattern of as-deposited PVP-CZTS sample shows amorphous in nature. The annealed PVP-CZTS sample revealed highly intensive peaks indicating the good crystalline nature. The calculated lattice parameters ($a$ = 5.44 Å, $b$ = 5.42 Å, $c$ = 10.89 Å) were well-matched with earlier reports.[4,12] The product obtained after annealing exhibited three strong peaks at $2\theta$ = 28:5, 47.3, and 56.2 corresponding to (112), (220), and (312) planes, respectively. The other three weak peaks at $2\theta$ = 32:36, 69.44, and 76.79° correspond to (200), (008), and (332) planes, respectively, of the tetragonal CZTS phase (JCPDS card 26-0575) (please see the Supporting Information, Table S1). Figure 1b shows the indexed XRD pattern for CA-CZTS nanofibers annealed at 450°C in nitrogen atmosphere. This pattern is also well-matched with pure phase kesterite CZTS (JCPDS 00-26-0575). However, the crystallinity of CA-CZTS sample is less compared to PVP-CZTS sample because of the nanocrystalline nature of CA-CZTS nanofibers. No secondary phases are detected in both PVP-CZTS and CA-CZTS samples, indicating that the deposited samples are highly phase-pure (Please see the Supporting Information, Table S2).

Figure 2a–d show FESEM micrographs of the prepared CZTS sample using PVP precursor at different magnifications. The low-magnification FESEM image shows fibrous network like CZTS nanofibers are covered throughout the surface. Moreover, the surface of CZTS nanofibers are quite smooth with 100–150 nm in diameter, which is confirmed by highly magnified FESEM image (Figure 2d). Figure 2e shows the FESEM image of PVP-CZTS after annealing in a nitrogen atmosphere, showing that the surface of nanofibers becomes rough and the diameter of the nanofibers has been reduced. Further, we have changed the electrospinning precursor. Figure 3a–d show FESEM images of CZTS nanofibers synthesized using CA precursor at different magnifications. Lower-magnification FESEM images show wirelike network of the CZTS nanofibers. The higher-magnification images clearly reveals that the deposited fibers having 30-40 nm in diameter (Figure 3d). After annealing the CA-CZTS nanofiber, the smooth surface has been transformed into a rough surface because of removal of CA (Figure 3e). Because of the good electrospinnability, cost effectiveness, and degree of substitution (DS) of PVP or CA polymers, they are commonly used as mesoporous templates for electrospinning. The high-voltage 9 kV (for PVP) or 15 kV (for CA) is sufficient for ejection of polymeric jet from syringe needle tip to collector.[28,32]

Figure 4a–c shows TEM micrographs of PVP-CZTS nanofibers sample deposited 9 kV. The fibers like nanostructure

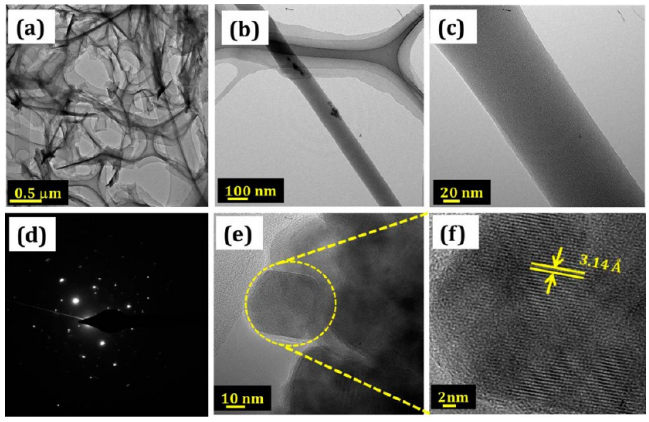


**Figure 4.** (a–c) TEM images of PVP-CZTS nanofibers at different magnifications, (d) SAED pattern, (e, f) HR-TEM images.

can be easily seen. From the TEM image, it is clear that the synthesized CZTS fibers are 100–150 nm diameter. The low-magnification image shows these nanofibers are quite long in the range of micrometers (Figure 4a). The crystallinity of the deposited nanofibers was determined from the selected area electron diffraction (SAED) patterns shown in Figure 4d. The SAED pattern of the PVP/CZTS nanofibers shows a spot pattern, which indicates a single-crystalline nature of the CZTS nanofibers. Images e and f in Figure 4 show HRTEM images of CZTS nanowire at different magnifications. The lattice spacing along the (112) plane indicated by yellow lines and found 3.14 Å is well consistent with the kesterite CZTS tetragonal ($I42m$) phase (JCPDS 26-0575).

Figure 5a–c shows TEM micrographs of CA-CZTS nanofibers deposited at 15 kV. The fiberlike nanostructures have diameters from 10 to 15 nm with micrometer scale in length. It is noted that the diameter of the CA assisted CZTS nanofiber is drastically reduced from 100 to 10–20 nm. It is well-known that the wire diameter decreased with increasing viscosity in electrospinning technique. Applied potential is also affecting onto electrospun nanofibers diameter. Here we have used 15 kV instead of 9 kV; therefore, the diameter of the CA-assisted CZTS nanofibers have been decreased drastically. This may be due to the greater expanded conformation of CA and good electrospinnability.[13] Figure 5d shows the SAED image of the CA-CZTS nanofibers, which is consistent with JCPDS no. 26-0575,

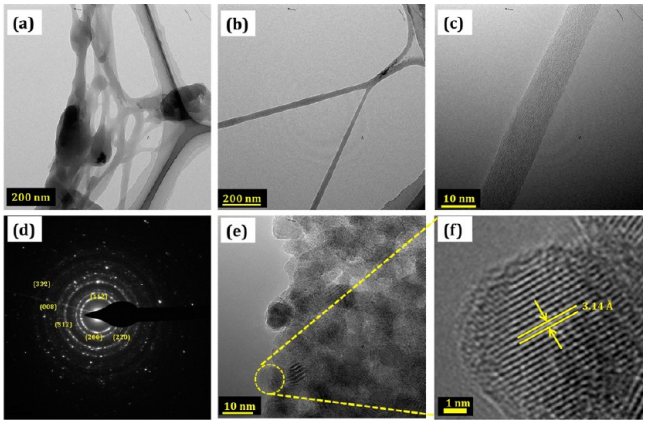


**Figure 5.** (a–c) TEM images of CZ-CZTS nanofibers at different magnifications, (d) SAED pattern, (e, f) HR-TEM images.

as it shows the (112), (200), (220), (312), (008), and (332) planes, and indicates that the nanofibers have a polycrystalline in nature. Images e and f in Figure 5 show the HRTEM micrographs of a CZTS nanofiber, and the spacing of the crystal lattice is 3.14 Å, which is consistent with the crystal lattice plane of kesterite CZTS along the (112) direction.

The elemental information of both the PVP and CA-assisted CZTS nanofibers were analyzed using an XPS (Figure 6). All four Cu, Zn, Sn, and S elements are present in XPS spectra. The Cu(2p) shows two peaks at 931.67 and 951.5 eV for Cu($2p_{3/2}$) and Cu($2p_{1/2}$) core levels respectively (Figure 6a). The separation between these two core levels is 19.83 eV, which is very close to the standard Cu(I) separation.[4] The Zn(2p) core level spectrum is located at 1021.34 eV and 1044.34 eV and corresponds to Zn($2p_{3/2}$) and Zn($2p_{1/2}$), respectively, and a peak splitting of 23 eV indicates the Zn(II) state (Figure 6b).[33] The Sn($2d_{5/2}$) and Sn($2d_{3/2}$) core level peak spectra were observed at 486.86 and 495.56 eV, respectively, with peak splitting at 8.7 eV confirming the Sn(IV) state as shown in (Figure 6c).[4] Furthermore ,the S(2p) curve fitting (160.71 and 162.14 eV) indicates confirmation of the $Cu_2ZnSnS_4$ phase.[4,21]

Figure 7 shows the optical absorption spectra of CZTS nanofibers dispersed in toluene solution and nature of optical transition were analyzed using well-known classical optical

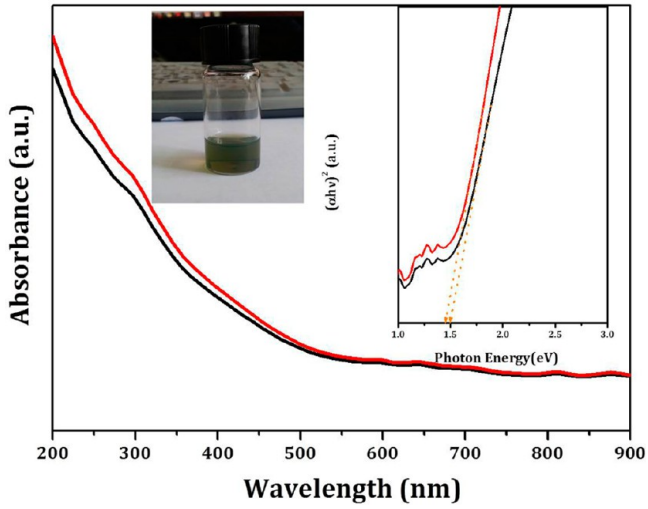


**Figure 7.** UV–vis spectra of PVP-CZTS and CA-CZTS nanofibers dispersed in toluene solution. Right hand inset shows the plot of $(\alpha h\nu)^2$ versus $h\nu$ (eV) for the nanocrystals. Left hand inset shows the photograph of well dispersed CZTS nanofibers in toluene solvent.

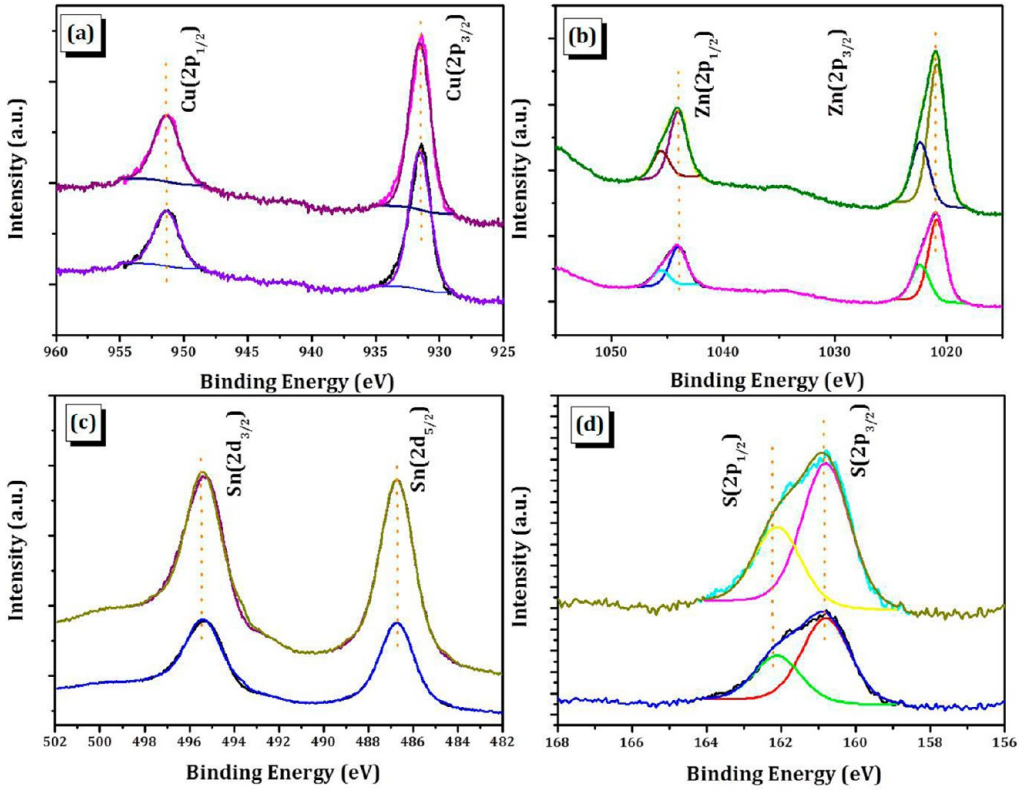


**Figure 6.** Core level (a) Cu (2p), (b) Zn (2p), (c) Sn (3d), and (d) S(2p) XPS spectra of the PVP-CZTS and CA-CZTS nanofibers.


dx.doi.org/10.1021/am404586n | ACS Appl. Mater. Interfaces 2014, 6, 1688–1696

equation.[34] Left side inset figure shows the photograph of well dispersed CZTS nanofibers. The calculated optical band gap energies for both PVP-CZTS and CA-CZTS sample are found 1.5 eV indicating pure phase $Cu_2ZnSnS_4$.[7,18] Figure 8 illustrates

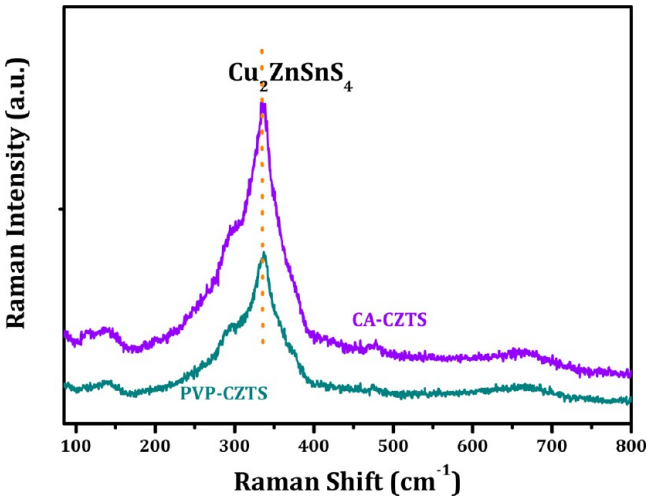


**Figure 8.** Micro-Raman spectra of PVP-CZTS and CA-CZTS nanofibers.

the typical micro-Raman spectra of the PVP-CZTS and CA-CZTS nanofibers annealed at 450 °C deposited by the electrospinning technique. The strong signal at 336 $cm^{-1}$ corresponds to single-phase quaternary $Cu_2ZnSnS_4$.[35−39] Other compounds and mixed-phase impurity peaks are not observed in the CZTS Raman spectra.

The current−voltage ($J$−$V$) characteristics were measured using Pt/FTO, PVP-CZTS/FTO, and CA-CZTS/FTO counter electrodes and N719-$TiO_2$/FTO working electrode separately. Figure 9 shows the $J$−$V$ characteristics of DSSC under

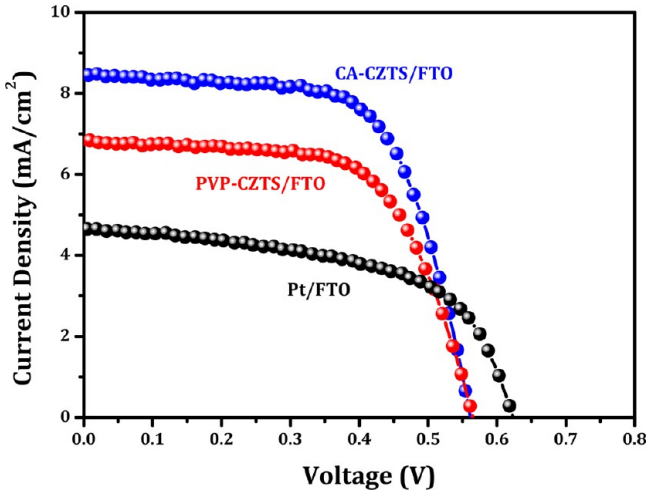


**Figure 9.** Current−voltage characteristics of the as-prepared dye-sensitized solar cells based on Pt, PVP-CZTS, and CA-CZTS counter electrodes.

illumination. The standard Pt/FTO counter electrodes based DSSC device shows: short circuit current density ($J_{SC}$) of 4.66 mA/$cm^2$, open circuit voltage ($V_{OC}$) of 0.623 V, fill factor (FF) of 0.57, and power conversion efficiency ($\eta$) of 1.72%. Replacing the Pt-coated FTO with the PVP-CZTS nanofiber counter electrodes, the $V_{OC}$ of the device decreases up to 0.577 V; however, the $J_{SC}$ and FF increases drastically 6.83 mA/$cm^2$ and 0.64, respectively. The conversion efficiency of PVP-CZTS/FTO-based counter electrode shows 3.10%. In the case of CA-CZTS/FTO-based counter electrode, the $J_{SC}$ increased significantly from 6.83 to 8.42 mA/$cm^2$. On the other hand, the $V_{OC}$ remains almost constant (0.574 V) for CA-CZTS sample. Scheme 2 shows the schematic representation of the N719-$TiO_2$

**Scheme 2. Schematic Representation of the N719-$TiO_2$ Working Electrode and CZTS Nanofiber Counter Electrode with Possible Electron Transport Mechanism**

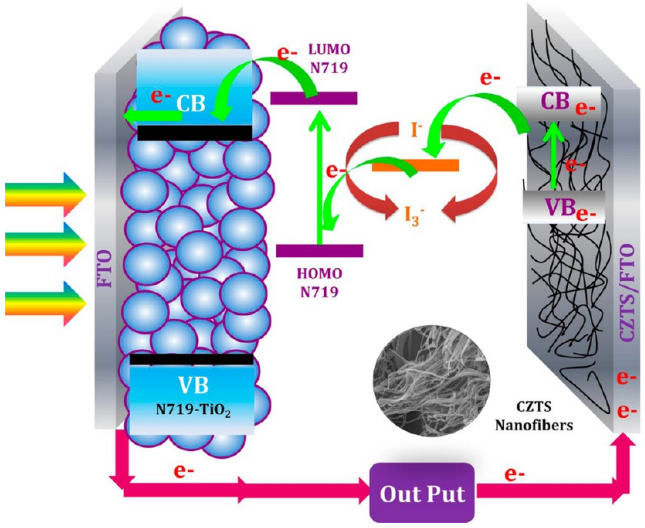


**Table 1. Photovoltaic Performance of the DSSC Devices with Respect to Different Counter Electrodes**

| counter electrode | $V_{oc}$ (V) | $J_{sc}$ (mA/$cm^2$) | FF (%) | $\eta$ (%) | $R_{sh}$ (Ω/$cm^2$) | $R_s$ (Ω/$cm^2$) |
|---|---|---|---|---|---|---|
| Pt/FTO | 0.623 | 4.66 | 57 | 1.72 | 5821 | 96 |
| PVP-CZTS/FTO | 0.577 | 6.83 | 64 | 3.10 | 9371 | 73 |
| CA-CZTS/FTO | 0.574 | 8.42 | 65 | 3.90 | 5323 | 69 |

working electrode and CZTS nanofiber counter electrode with possible electron transport mechanism. Table 1 represents the summary of photovoltaic performance of DSSC devices based on different counter electrodes. From Table 1, it is clear that the CA-CZTS-based device shows the lowest series resistance ($R_S$), 69 Ω/$cm^2$, compared to both Pt/FTO (96 Ω/$cm^2$) and PVP-CZTS/FTO (73 Ω/$cm^2$) counter electrodes. It is well-known that the $J_{SC}$ of the DSSC solar cells depends on the $R_S$ of the devices. Generally, lower $R_S$ is favorable for higher $J_{SC}$ and can be calculated using inverse slop of the JV curves. From morphological studies it is clear that the diameter of CA-CZTS sample is lower compared to PVP-CZTS sample. The smaller nanofibers provide large surface area and effective path for electrons transportation and redox reaction. This effect results in a more smooth and efficient electron transport in the CA-CZTS/FTO electrodes. Therefore, the CA-CZTS/FTO counter electrode offers lower interfacial recombination between the counter electrode and electrolyte[40] results in higher conversion efficiency compared to PVP-CZTS/FTO and Pt/FTO based counter electrodes. Moreover, the current density of the DSSCs depends on the Rs of the devices. It is well-known that the lower $R_S$ offers higher current density. Therefore, the CA-CZTS/FTO counter electrode-based DSSC device shows the lowest $R_S$ values,


dx.doi.org/10.1021/am404586n | ACS Appl. Mater. Interfaces 2014, 6, 1688−1696

which is favorable for higher current density (8.42 mA/cm$^2$) and conversion efficiency (3.90%) compared to PVP-CZTS/FTO and Pt/FTO counter electrodes. The above results revealed that PVP-CZTS as well as CA-CZTS nanofibers work as an effective counter electrode material in DSSCs.

To confirm the reason behind this, we have recorded the electrochemical impedance spectroscopy (EIS). Figure 10 shows

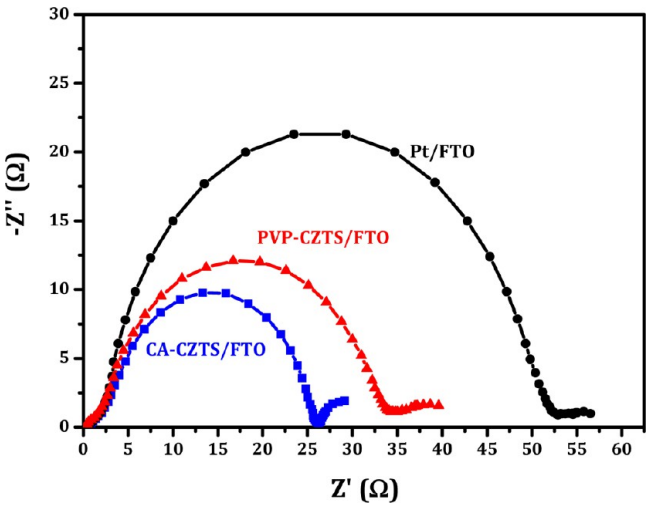


**Figure 10.** Electrochemical impedance spectra (EIS) of as-prepared dye sensitized solar cells based on Pt/FTO, PVP-CZTS/FTO, and CA-CZTS/FTO counter electrodes.

the EIS spectra of the $TiO_2$-based DSSCs devices with different counter electrodes. All EIS spectra were recorded at a forward 0.7 V bias of the open-circuit voltage with an ac potential amplitude of 10 mV and a frequency range from 0.1 Hz to $1 \times 10^5$ Hz. In the impedance spectrum, the first semicircle in the high-frequency region indicates the charge-transfer resistance ($R_{ct}$) at the counter electrode and redox couple ($I^-/I_3^-$) at the interface. The second semicircle in the low-frequency region indicates the charge-transfer process at the $TiO_2$/N-719-Dye/electrolyte interface.[41] From Nyquist plots, it is clear that the $R_{ct}$ value is decreased for the CA-CZTS/FTO counter electrode compared to other Pt/FTO and PVP/FTO counter electrodes. Generally series resistance ($R_s$) in DSSCs is depend on sheet resistance of the FTO substrate, charge transfer resistance ($R_{ct}$) and diffusion resistance ($R_{diff}$) between counter electrode and electrolyte.[40,41] From the EIS spectra (Figure 10), it is clear that CA-CZTS-based counter electrode shows the lowest $R_{ct}$ values compared to other devices, indicating a better catalytic property and lower recombination at the interfaces. Such decrement in $R_{ct}$ is favorable for efficient charge transportation and results in higher photovoltaic performance.

## 4. CONCLUSIONS

In summary, we have successfully synthesized PVP- and CA-assisted CZTS nanofibers via an electrospinning technique. Surface morphology reveals that the PVP-assisted CZTS nanofibers have a smooth surface with 100−150 nm diameters, whereas CA-assisted samples show 10−20 nm diameters. The XRD and TEM results revealed that the PVP-assisted CZTS nanofibers are single kesterite crystalline in nature, whereas CA-assisted CZTS nanofibers are kesterite polycrystalline in nature. Optical properties showed that, 1.5 eV direct band gap energy indicating these materials are useful for CZTS-based, low-cost solar cell application. Finally, the fabricated Pt/FTO, PVP-CZTS/FTO, and CA-CZTS/FTO counter electrode based DSSCs shows 1.72, 3.10, and 3.90 % conversion efficiency respectively. The EIS results revealed that CA-CZTS counter electrode shows lower Rs, which is favorable for lower recombination rate and higher conversion efficiency of DSSCs. The nanofibrous CZTS counter electrodes show the potential to convert Pt/FTO-based DSSCs to earth-abundant element-based counter electrodes.

## ■ ASSOCIATED CONTENT

### Supporting Information

Thermogravimetric analysis (TGA) of PVP-CZTS and CA-CZTS, cyclic voltammograms (CV) of PVP-CZTS and CA-CZTS counter electrodes, and XRD data analysis of PVP-CZTS and CA-CZTS samples. This material is available free of charge via the Internet at http://pubs.acs.org/.

## ■ AUTHOR INFORMATION

### Corresponding Author

*E-mail: hongck@chonnam.ac.kr.

### Notes

The authors declare no competing financial interest.

## ■ ACKNOWLEDGMENTS

This research was supported by the Basic Science Research Program through the National Research Foundation of Korea (NRF) funded by the Ministry of Education (NRF-2009−0094055).

## ■ REFERENCES

(1) Ito, K.; Nakazawa, T. *Jpn. J. Appl. Phys.* **1988**, *27*, 2094−2097.
(2) Tanaka, T.; Nagatomo, T.; Kawasaki, D.; Nishio, M.; Guo, Q.; Wakahara, A.; Yoshida, A.; Ogawa, H. *J. Phys. Chem. Solids* **2005**, *66*, 1978−1981.
(3) Mali, S. S.; Shinde, P. S.; Betty, C. A.; Bhosale, P. N.; Oh, Y. W.; Patil, P. S. *J. Phys. Chem. Solids* **2012**, *73*, 735−740.
(4) Mali, S. S.; Patil, B. M.; Betty, C. A.; Bhosale, P. N.; Oh, Y. W.; Jadkar, S. R.; Devan, R. S.; Ma, Y. R.; Patil, P. S. *Electrochim. Acta* **2012**, *66*, 216−221.
(5) Guo, Q.; Kim, S. J.; Kar, M.; Shafarman, W. N.; Birkmire, R. W.; Stach, E. A.; Agrawal, R.; Hillhouse, H. W. *Nano Lett.* **2008**, *8*, 2982−2987.
(6) Katagiri, H.; Jimbo, K.; Maw, W.S.; Oishi, K.; Yamazaki, M.; Araki, H.; Takeuchi, A. *Thin Solid Films* **2009**, *517*, 2455−2460.
(7) Repins, I.; Contreras, M.A.; Egaas, B.; DeHart, C.; Scharf, J.; Perkins, C.L.; To, B.; Noufi, R. *Prog. Photovolt.* **2008**, *16*, 235−239.
(8) Scragg, J.J.; Dale, P.J.; Peter, L.M. *Electrochem. Commun.* **2008**, *10*, 639−642.
(9) Shavel, A.; Cadavid, D.; Ibáñez, M.; Carrete, A.; Cabot, A. *J. Am. Chem. Soc.* **2012**, *134*, 1438−1441.
(10) Seboui, Z.; Cuminal, Y.; Kamoun-Turki, N. *J. Renewable Sustainable Energy* **2013**, *5*, 023113.
(11) Sarswat, P. K.; Free, M. L. *Phys. Status Solidi (a)* **2011**, *208*, 2861−2864.
(12) Hsu, K. C.; Liao, J. D.; Yang, J. R.; Fu, Y. S. *CrystEngComm* **2013**, *15*, 4303−4308.
(13) Chen, L. J.; Chuang, Y. J. J. *Power Sources* **2013**, *241*, 259−265.
(14) Mali, S. S.; Kim, H. J.; Shim, C. S.; Patil, P. S.; Hong, C. K. *Phys. Status Solidi RRL* **2013**, *7*, 1050−1054.
(15) Hillhouse, H. W.; Beard, M. C. *Curr. Opin. Colloid Interface Sci.* **2009**, *14*, 245−259.
(16) Mitzi, D. B.; Gunawan, O.; Todorov, T. K.; Wang, K.; Guha, S. *Sol. Energy Mater. Sol. Cells* **2011**, *91*, 1421−1425.

(17) Ennaoui, A.; Lux-steiner, M.; Weber, A.; Abou-ras, D.; Kötschau, I.; Schock, H.; Schurr, R.; Holzing, A.; Jost, S.; Hock, R.; Voß, T.; Schulze, J.; Kirbs, A. *Thin Solid Films* **2009**, *517*, 2511−2514.
(18) Habas, S. E.; Platt, H. A. S.; van Hest, M. F. A. M.; Ginley, D. S. *Chem. Rev.* **2010**, *110*, 6571−6594.
(19) Guo, Q.; Ford, G. M.; Yang, W.-C.; Walker, B. C.; Stach, E. A; Hillhouse, H. W.; Agrawal, R. *J. Am. Chem. Soc.* **2010**, *132*, 17384−17386.
(20) Lin, X.; Kavalakkatt, J.; Kornhuber, K.; Abou-Ras, D.; Schorr, S.; Ch. Lux-Steiner, M.; Ennaoui, A. *RSC Adv.* **2012**, *2*, 9894−9898.
(21) Shin, B.; Gunawan, O.; Zhu, Y.; Bojarczuk, N. A.; Chey, S. J.; Guha, S. *Prog. Photovolt.* **2013**, *21*, 72−76.
(22) Guo, Q.; Ford, G. M.; Yang, W.C.; Walker, B. C.; Stach, E. A; Hillhouse, H. W.; Agrawal, R. *J. Am. Chem. Soc.* **2010**, *132*, 17384−17386.
(23) Todorov, T. K.; Tang, J.; Bag, S.; Gunawan, O.; Gokmen, T.; Zhu, Y.; Mitzi, D. B. *Adv. Energy Mater.* **2013**, *3*, 34−38.
(24) Guo, Q.; Hillhouse, H. W.; Agrawal, R. *J. Am. Chem. Soc.* **2009**, *131*, 11672−11673.
(25) Shavel, A.; Arbiol, J.; Cabot, A. *J. Am. Chem. Soc.* **2010**, *132*, 4514−4515.
(26) Jung, Y. H.; Park, K. H.; Oh, J. S.; Kim, D. H.; Hong, C. K. *Nanoscale Res. Lett.* **2013**, *8*, 37−42.
(27) Song, W.; Wang, Y.; Zhao, B. *J. Phys. Chem. C* **2007**, *111*, 12786−12791.
(28) Mali, S. S.; Kim, H. J.; Jang, W. Y.; Park, H. S.; Patil, P. S.; Hong, C. K. *ACS Sustainable Chem. Eng.* **2013**, *1*, 1207−1213.
(29) Mali, S. S.; Kim, H. J.; Shim, C. S.; Patil, P. S.; Kim, J. H.; Hong, C. K. *Sci. Rep.* **2013**, *3*, 3004.
(30) O'Regan, B.; Grätzel, M. *Nature* **1991**, *353*, 737−740.
(31) Mali, S. S.; Shinde, P. S.; Betty, C. A.; Bhosale, P. N.; Lee, W. J.; Patil, P. S. *Prog. Photovolt.: Res. Appl.* **2012**, DOI: 10.1002/pip.2295.
(32) Fischer, S.; Thümmler, K.; Volkert, B.; Hettrich, K.; Schmidt, I.; Fischer, K. *Macromol. Symp.* **2008**, *262*, 89−96.
(33) Liu, Y.; Yao, D.; Shen, L.; Zhang, H.; Zhang, X.; Yang, B. *J. Am. Chem. Soc.* **2012**, *134*, 7207−7210.
(34) Pankove, J.I. *Optical Processes in Semiconductors*, Dover, New York, 1976.
(35) Singh, A.; Geaney, H.; Laffir, F.; Ryan, K. M. *J. Am. Chem. Soc.* **2012**, *134*, 2910−2913.
(36) Woo, K.; Kim, Y.; Moon, J. *Energy Environ. Sci.* **2012**, *5*, 5340−5345.
(37) Altosaar, M.; Raudoja, J.; Timmo, K.; Danilson, M.; Grossberg, M.; Krustok, J.; Mellikov, E. *Phys. Status Solidi (a)* **2008**, *205*, 167−170.
(38) Fernandes, P. A.; Salome, P. M. P.; da Cunha, A. F. *Thin Solid Films* **2009**, *517*, 2519−2523.
(39) Liu, F.; Li, Y.; Zhang, K.; Wang, B.; Yan, C.; Lai, Y.; Zhang, Z.; Li, J.; Liu, Y. *Sol. Energy Mater. Sol. Cells* **2010**, *12*, 2431−2434.
(40) Xu, J.; Yang, X.; Yang, Q. D.; Wong, T. L.; Lee, C. S. *J. Phys. Chem. C* **2012**, *116*, 19718−19723.
(41) Ramasamy, E.; Lee, W. J.; Lee, D. Y.; Song, J. S. *Electrochem. Commun.* **2008**, *10*, 1087−1089.